Arabian Journal of Chemistry (2020) 13, 4966–4977

King Saud University

Arabian Journal of Chemistry

www.ksu.edu.sa
www.sciencedirect.com

ORIGINAL ARTICLE

Sunlight assisted photocatalytic degradation of organic pollutants using g-C_3N_4-TiO_2 nanocomposites

Radhakrishna S. Sutar [a], **Rani P. Barkul** [a], **Sagar D. Delekar** [b], **Meghshyam K. Patil** [a,*]

[a] *Department of Chemistry, Dr. Babasaheb Ambedkar Marathwada University, Aurangabad, Sub-campus, Osmanabad 413 501, MS, India*
[b] *Department of Chemistry, Shivaji University, Kolhapur 416004, MS, India*

Received 9 July 2019; accepted 21 January 2020
Available online 28 January 2020

KEYWORDS

Nanocomposites;
TiO_2;
g-C_3N_4;
Photocatalytic degradation;
Bisphenol A;
Brilliant green

Abstract The photocatalytic degradation of environmentally non-benign, toxic organic pollutants such as bisphenol A (BPA), brilliant green (BG), or mixture of dyes have been carried out using g-C_3N_4-TiO_2 (GNT) nanocomposites. The GNT nanocomposites were synthesized by using hydrothermal method with different compositions and these nanocomposites were characterized using the different techniques. X-ray diffraction revealed that the anatase phase of TiO_2 has been retained in composites; while characteristic reflection of g-C_3N_4 at 27.07° (d = 3.22 Å) is not observed due to its lower content in the nanocomposites. Raman spectra confirms the formation of composites between TiO_2 with g-C_3N_4. Furthermore nano-scale dimensions of the bare or composites have been proved by FE-SEM and HR-TEM analysis. X-ray photoelectron spectroscopy (XPS) shows the presence of C, N, Ti and O as a constituents, with peaks due to C—C, N—C=N of g-C_3N_4. Among the different nanocomposites, g-C_3N_4-TiO_2 catalyst having 30% g-C_3N_4 and 70% TiO_2 in molar proportion (i.e. 30-GNT) is exhibiting the highest efficiency for degradation of the different dyes in correlation to its higher surface area, lower optical band gap as well as more visible-light absorption (i.e., $\lambda > 400$ nm) in the electromagnetic spectrum.

1. Introduction

Among the various environmental issues, the contamination of toxic waste into the atmosphere is one of the major challenge of the globe and it forms the various ecological problems to be very harmful to living organisms. The majority of environmental pollutants are the carcinogenic natured and non-degradable coloured dye effluents, to be discharged by the textile, leather, printing and paper industries, etc. Most of the industries use color dyes for uplifting the features of goods

* Corresponding author.
E-mail address: meghshyam_patil@yahoo.com (M.K. Patil).
Peer review under responsibility of King Saud University.

ELSEVIER Production and hosting by Elsevier

https://doi.org/10.1016/j.arabjc.2020.01.019

and hence unused or bare colorants during the industrial processes are discharged in waterbodies or air (Sankar et al., 2014). In addition, another group of compounds referred as chemical contaminants of emerging concern (CEC) is also responsible for water pollution. These CECs includes pharmaceuticals, personal care products and industrial chemicals etc. Industrial CECs have the largest and most diverse set of chemicals, some of them are organophosphate esters, synthetic additives to plastics such as phthalates, bisphenol A (BPA), benzotriazoles and poly- and perfluoroalkyl substances (PFASs) etc (Program, 2017). Now-a-days, several research groups from all over the world are focused on the degradation of the dyes (or colorants) and CECs by different strategies. Among them, advanced oxidation process (AOP) is one of the process used to treat the polluted water for removing the contaminants. In comparison to the different oxidising agents used in AOP, nanocrystalline semiconductor based photocatalysts having overriding advantages include ease separation, higher catalytic rate, ability towards removal of a wide range of inorganic and organic pollutants (Kubacka et al., 2011), working without any external reagents and mostly working under sunlight, etc.

Particularly, photocatalytic TiO_2 materials commonly used in AOP studies due to its overall cost, generation of reactive oxygen species, etc. However, TiO_2 has large band gap of 3.2 eV and the high recombination rate of electron/hole pairs; which retards its practical applications in visible light activated photocatalytic studies (Fujishima and Honda, 1972; Henderson, 2011; Hoffmann et al., 1995; Marugán et al., 2006; Pan et al., 2012; Yang et al., 2012). To overcome these drawbacks, there is dire need to modify the bare TiO_2 for tuning optical band gap to absorb visible light as well as for increasing the separation charge carriers to increase the photocatalytic performance. In view of this, many strategies have been imparted, includes metal or non-metal doping (Barkul et al., 2017; Ge et al., 2013), dye-sensitization (Dai et al., 2014; Takanabe et al., 2010), surface modification by controlling morphology (Ma et al., 2016b; Zhao et al., 2015), constructing heterojunction (Gondal et al., 2015; Xing et al., 2014), semiconductor-coupling (Sun et al., 2010a), etc. Among these strategies, making nanocomposite (NC) with other material has been proved to be an impactful method to enhance the photocatalytic activity due to its significant impact on the modification of electronic and optical properties of material (Fu et al., 2005; Li et al., 2007).

Graphite-like carbon nitride (g-C_3N_4) is the best material for making nanocomposite with TiO_2 because of the interfacial connection between these two components as well as delocalized conjugated structure leads ease electrons transfer and hence this retards the recombination rate of the charge carriers (Ma et al., 2016a). In addition, g-C_3N_4 is also metal-free photocatalyst with band gap of 2.7–2.8 eV, which having high thermal, chemical stability (Jun et al., 2013; Schwinghammer et al., 2014; Yang et al., 2013) and it has been used as heterostructure in several applications such as photocatalytic NO removal, H_2 production, hydrocarbon oxidation, etc. (Cui et al., 2020; Ding et al., 2011; Liao et al., 2020; Samanta et al., 2014; Wang et al., 2018; Xiong et al., 2018). The synergetic of electron transfer as well as optical absorption behaviour, g-C_3N_4 would boost the opto-electrical properties of bare TiO_2 materials and hence the NCs between these two enhances the visible light driven photocatalytic studies efficiently (Wang et al., 2011). Though, the photocatalytic activity of g-C_3N_4 is restrained by the fast recombination rate of the photo-generated electron hole pairs and the narrow excitation wavelength range of photocatalysts (Shao et al., 2016). The various methods have been used to prepare g-C_3N_4/TiO_2 NC such as thermal transformation method (Sridharan et al., 2013), ball milling method (Zhou et al., 2015) and so on. Taking into these considerations, in this present work, we have developed a facile and reproducible strategy for preparing GNT NCs by employing hydrothermal technique. These prepared NCs were characterized by most sophisticated techniques such as X-ray diffraction spectroscopy (XRD), fourier transform infrared spectroscopy (FTIR), scanning electron microscopy (SEM), energy-dispersive X-ray spectroscopy (EDX), high resolution transmission electron microscopy (HRTEM), UV–Visible spectroscopy (UV–Visible), X-ray photoelectron spectroscopy (XPS), and Raman spectroscopy, etc. The result reveals the formation of g-C_3N_4-TiO_2 NCs by deposition of uniform TiO_2 nanoparticles on to the surface of g-C_3N_4. The photocatalytic activity of these NCs have been tested for degradation of CEC bisphenol A (BPA), coloured dye brilliant green (BG) and mixture of three dyes namely brilliant green, methylene blue and methyl orange under direct sun light irradiation. The prepared NCs have shown significant enhancement in photocatalytic activity than pure TiO_2 and g-C_3N_4. Furthermore, effect of concentration of dye solution, pH of solution and amount of catalyst loading has been tested for degradation of brilliant green dye.

2. Experimental procedure

2.1. Preparation of catalysts

Synthesis of GNT NCs has been carried out by using hydrothermal method in the different molar ratio (such as 15:85, 30:70 of g-C_3N_4 and TiO_2 denoted as 15-GNT and 30-GNT). Also, nanocomposite has been synthesized by one more method, directly mixing hydrothermally formed TiO_2 and g-C_3N_4 before calcination and abbreviated as M-GNT. Details of catalyst preparation have been discussed in this section.

2.1.1. Preparation of g-C_3N_4

g-C_3N_4 was synthesized by using reported method (Zhang et al., 2017). In which, urea and thiourea was added in ethanol by continuous stirring at 80 °C for 1 h. This mixture was recrystallized by evaporation of ethanol. The obtained powder was heated at the rate of 5 °C/min and maintained at 400 °C for 2 h in an alumina crucible with a cover in air. Thus yellowish powder was obtained.

2.1.2. Preparation of TiO_2

Glacial acetic acid (2 ml) and ethanol (60 ml) were taken in 250 ml beaker and stirred continuously for 30 min. To this, titanium tetra-isopropoxide (7 ml) and water (2 ml) was added and solution was stirred for 30 min. at room temperature. This reaction mixture was transferred into a stainless steel autoclave and temperature maintained at 150 °C for 20 h. After hydrothermal treatment, the solution was cooled; obtained precipitate was filtered and washed with distilled water. Finally the compound was dried at 80 °C and calcined at 450 °C for 4 h.

2.1.3. Preparation of GNT nanocomposites

Glacial acetic acid (2 ml) was slowly added into the ethanol (60 ml) with vigorous stirring for 30 min. To this, titanium tetra-isopropoxide (5.95 ml) and then water (2 ml) was added and stirred for 30 min. Furthermore, synthesized g-C_3N_4 (0.246 gm) was added into this reaction mixture with appropriate molar ratio and solution was transferred into a stainless steel autoclave and maintained at 150 °C for 20 h. After hydrothermal treatment, the solution was cooled and obtained precipitate was filtered, washed with distilled water and dried at 80 °C. Finally compound calcined at 450 °C for 4 h. By applying this protocol, we have synthesized two nanocompos-

ites 15-GNT and 30-GNT having molar proportion 15: 85 and 30: 70 of g-C_3N_4 and TiO_2 respectively.

2.1.4. Preparation of M-GNT

The preparedg-C_3N_4 and TiO_2 (before calcination prepared by hydrothermal treatment) in the molar ratio 15:85, were mixed thoroughly. The obtained mixture was dried at 80 °C and calcined at 450 °C for 4 h.

2.2. Characterization

X-ray diffraction (XRD) spectra of the all samples were recorded by using Regaku diffractometer with Cu Ka (1.5418 Å). The diffraction data have been collected in the range of 10° to 80° with scan rate 0.2/min. FTIR spectra of the NCs were recorded on Thermo Nicolet Nexus 670 model in the range of 400–4000 cm^{-1}. UV–visible absorption spectrum of NCs were recorded in the range of 200–800 nm by using Bio-Age UV–VIS spectrophotometer. The morphology and elemental composition of the material was analysed by using field-emission scanning electron microscope (FE-SEM) with energy-dispersive X-ray spectroscopy (EDX). Furthermore, HR-TEM images were recorded on a PHILIPS CM200 field emission transmission electron microscope having operating voltages of 20–200 kV with resolution of 2.4 Å. XPS measurement of the prepared NCs were recorded on a Shimadzu (ESCA 3400) spectrometer by using Mg Kα (1253.6 eV) radiation as the excitation source. Raman analysis of photocatalysts were carried out on Nicolet FT-Raman 960 spectrometer with a range of 4000–100 cm^{-1} and a spectral resolution of 2 cm^{-1} using the 1064 nm exciting line (~600 mV).

2.3. Photocatalytic degradation

The photocatalytic activity of the GNT and bare TiO_2 has been tested on the degradation of organic pollutants such as BPA, BG and mixed dyes (20.0 mg/L) in aqueous solution under direct sunlight. Also various parameters of degradation reaction, such as concentration of dye, amount of catalysts, pH of dye solution, etc. has been studied. The pH of the dye solution was adjusted by adding few drops of NaOH or HCl (1 N).

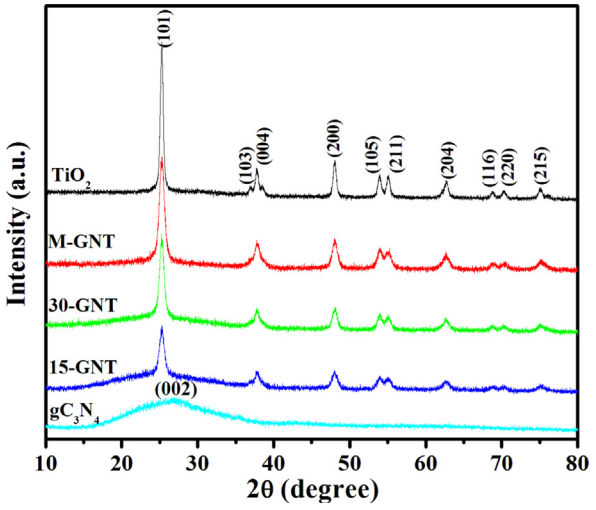

Fig. 1 XRD spectra of bare TiO_2, bare g-C_3N_4 and GNT nanocomposites.

2.3.1. Photocatalytic degradation of BG, BPA and mixture of dyes

The 200 ml (20 mg/L) BG solution was taken in 250 ml round bottom flask and 100 mg prepared catalyst was added. This assembly was stirred in dark at room temperature for 30 min to reach the adsorption desorption equilibrium and then kept in sunlight directly. Samples were taken after given time intervals and centrifuged for analysis. Absorbance of obtained samples were measured at wavelength 200–800 nm. Also the colour of dye solution decreased with time illumination. Furthermore, similar protocol was used for degradation of BPA and for mixture of dyes (a solution of methyl orange, methylene blue, BG).

3. Results and discussion

3.1. X-ray diffraction study

XRD patterns of all samples are shown in Fig. 1. Diffraction pattern of pure g-C_3N_4 shows strongest broad (0 0 2) reflection peak at 27.07° (d = 3.22 Å) matches with reported XRD data of g-C_3N_4 (Guo et al., 2003). Diffraction patterns of GNT and pure TiO_2 correspond to anatase phase of TiO_2 (JCPDS-211272); which reveals that bare TiO_2 or GNT retain tetragonal structure only. In the diffraction patterns of GNT, with increasing the percentage of g-C_3N_4 in the nanocomposite, diffraction peaks become broad with decrease in intensity. The structural parameters of these NCs and bare TiO_2 are listed in Table 1. The average crystallite size of 30-GNT is 11.42 nm, 15-GNT is 12.22 nm, M-GNT is 18.24 nm, whereas pure TiO_2 having crystallite size 20.13 nm.

3.2. Raman spectra

Raman spectra of pure TiO_2 and composite 30-GNT in the range of 50–800 cm^{-1} is shown in Fig. 2. Here, Raman spectra were used to approve the attachment TiO_2 with g-C_3N_4 in the prepared catalyst. Five spectral bands of TiO_2 were observed in GNT and these bands are at ~144 cm^{-1} (strong band, E_g), ~198 cm^{-1} (E_g), ~399 cm^{-1} (B_{1g}), 514 cm^{-1} (A_{1g} + B_{1g}), and 638 cm^{-1} (E_g). All these bands are the characteristic bands for anatase phase of TiO_2. These observed peaks were assigned to the Ti-O-Ti network structure of TiO_2. When the TiO_2 nanoparticles attached to g-C_3N_4, there is a considerable not only increase in peak broadening but also decrease in intensity of characteristic bands; which confirms a strong chemical interaction between both components. A spectrum of 30-GNT composite exhibits the characteristics bands of TiO_2 and in addition, a new peak has been observed at ~482 cm^{-1} due to g-C_3N_4 (Troppová et al., 2018). Furthermore, the strongest intensity band of TiO_2, which is at 144 cm^{-1}, has been decreased in the prepared composite, confirms the strong interaction of TiO_2 with g-C_3N_4 rather than existing purely as a mixture of both.

Table 1 Structural parameters of bare TiO_2, composites M-GNT, 30-GNT and 15-GNT.

Catalysts	Standard d value	Observed d value	hkl plane	Cell parameters			Crystallite Size (nm)
				a(Å)	c(Å)	V(Å^3)	
TiO_2	3.52	3.52	(1 0 1)	3.76	9.48	134.02	20.13
	2.37	2.37	(0 0 4)				
	1.33	1.33	(2 2 0)				
M-GNT	3.52	3.52	(1 0 1)	3.76	9.49	134.16	18.24
	2.37	2.37	(0 0 4)				
	1.33	1.33	(2 2 0)				
30-GNT	3.52	3.52	(1 0 1)	3.76	9.51	134.30	11.42
	2.37	2.37	(0 0 4)				
	1.33	1.33	(2 2 0)				
15-GNT	3.52	3.52	(1 0 1)	3.76	9.49	134.16	12.22
	2.37	2.37	(0 0 4)				
	1.33	1.33	(2 2 0)				

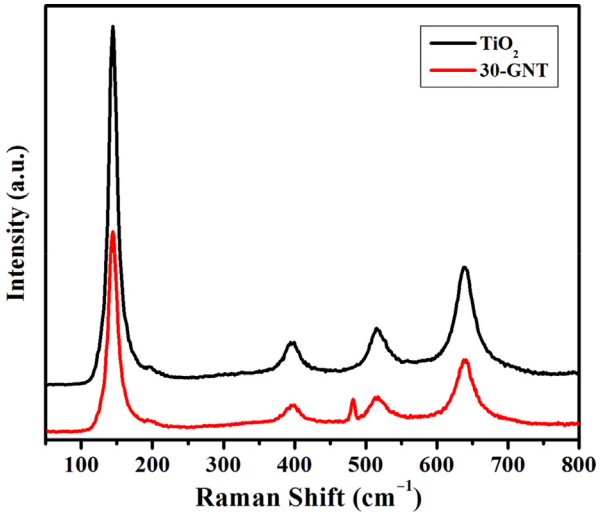

Fig. 2 Raman spectra of pure TiO_2 and 30-GNT composite.

3.3. UV–Visible absorption study

UV–visible absorption spectra of the representative samples are shown in Fig. 3(a). It is seen that the stronger absorption edge is red shifted towards the higher wavelength than that of bare TiO_2. It also reveals that the optical absorption of NCs is observed in the visible region of electromagnetic spectrum. This is attributed to matchable optical band levels of TiO_2 with g-C_3N_4. In the nanocomposite, the g-C_3N_4 would perform the role of a photo-sensitizer and responsible to extend the absorption of TiO_2 photocatalyst to the range of visible light through electron transfer as shown in Fig. 4. This figure also reveals that the charge carriers are transferred from LUMO of g-C_3N_4 (−2.4 eV) to conduction band of TiO_2 (−4.2 eV) (Troppová et al., 2018). To know the optical band gap of the samples, a graph of $h\upsilon$ vs $(\alpha h\upsilon)^2$ is plotted and shown in Fig. 3(b). The band gap range of prepared composites is from ~2.9 eV to 3.16 eV, whereas bare TiO_2 having band gap 3.3 eV (Fig. 3(b)).

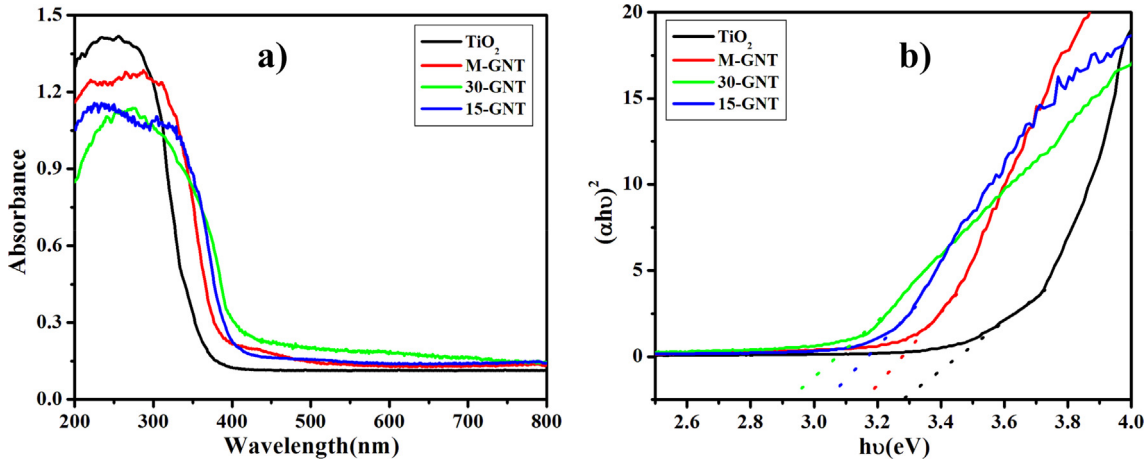

Fig. 3 (a) UV–Visible absorption spectra and (b) plot of hυ vs $(\alpha h\upsilon)^2$ of GNTs and bare TiO_2.

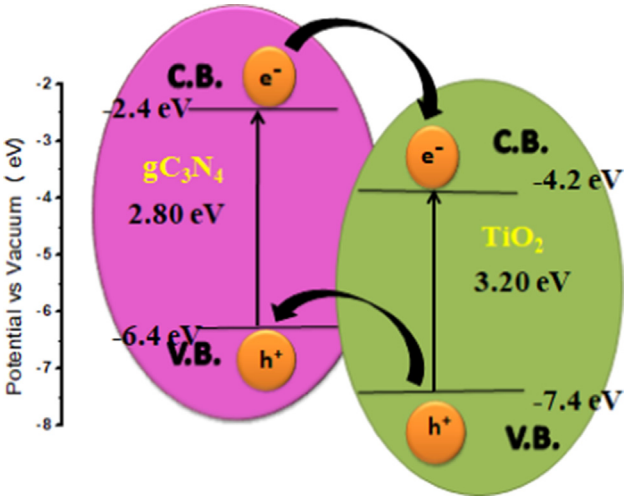

Fig. 4 Possible schematic representation of mechanism of GNT catalyst.

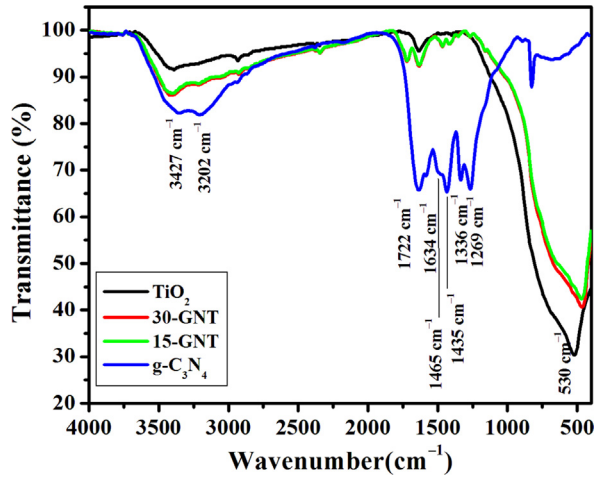

Fig. 5 FT-IR spectra of the 30-GNT, 15-GNT, g-C_3N_4 and bare TiO_2.

3.4. FT-IR studies

FT-IR spectra of all samples are shown in Fig. 5. The patterns of all GNT are similar and all these patterns consist of the peaks corresponding to the anatase TiO_2 as well as g-C_3N_4. All FT-IR spectra show the bands at 1722, 3202 and 3247 cm^{-1}; due to the stretching and deformation modes of NH_2 group, while a peak at 1634 cm^{-1} is due to stretching C-N bond and also shows good crystallinity of g-C_3N_4 (Liu et al., 2011; Troppová et al., 2018). While other bands at 1336, 1269 cm^{-1} corresponds to C—N (Zhou et al., 2014). Also the bands at 1435, 1465 cm^{-1} attributed due to s-triazine ring (Sun et al., 2010b).

In addition, the spectrum of pure TiO_2 and GNT also shows a broad band in range of 453–973 with sharp tip at 530 cm^{-1} attributed due to O—Ti—O bonding in anatase TiO_2 (Barkul et al., 2017). The peak at 1630 cm^{-1} and broad bands at 3397 cm^{-1} correspond to bending and stretching vibrations of —OH group respectively and appear due to physisorbed water molecule present on the TiO_2 surface. Surface hydroxylation is more in GNT samples than the pure TiO_2, which is more capable to reflect through more percentage transmittance at 3427 cm^{-1} in the IR spectrum and results in efficient photodegradation activity of GNT samples.

3.5. Field emission scanning electron microscopy (FESEM) and EDAX measurements

EDAX spectrum and FE-SEM images of representative samples are shown in Fig. 6. FE-SEM images reveals the formation of agglomerated nano-crystalline nature of the bare TiO_2 as well as GNT NCs with average grain size 500 nm to 10 μm. Whereas EDAX patterns of all representative GNT and TiO_2 provides useful information of elemental composition of synthesized materials. These EDAX spectrums show the peak of C, N, Ti and O in the samples.

3.6. High-resolution transmission electron microscopy (HRTEM)

The structural properties of prepared material 30-GNT catalyst were further investigated by using HR-TEM spectroscopy. Clear lattice fringes were obtained for both 15-GNT and 30-GNT nanomaterial as shown in Fig. 7(a, b, c). Both the HRTEM image shows well anatase crystalline compound and distances (d) of crystal lattice fringes is 0.352 nm which is corresponding to the spacing of (1 0 1) lattice plane of the anatase TiO_2 (JCPDS 211272). Also, area of g-C_3N_4 and TiO_2 has been shown in Fig. 7(b, c). The selected area electron diffraction (SAED) pattern of 30-GNT NC has been shown in Fig. 7(d), confirms the anatase phase of TiO_2, which is in good agreement with XRD results. The brightness and intensity of polymorphic rings in SAED pattern, reveals the well crystalline nature of nanocomposite. The average crystalline size of the composite was calculated from XRD is ~12 nm is also matches with HR-TEM results.

3.7. X-ray photoelectron spectroscopy

XPS measurements were taken for the analysis of chemical states of element and bond nature of prepared nanocomposite 30-GNT and shown in Fig. 8. From the Fig. 8(b) three peaks are positioned at 283.3, 284.8 and 287.1 eV; the peaks situated at 283.3 and 284.8 eV can be ascribed to the C—C, and the peak at ~287.1 eV is corresponds to C—O bond due to adsorbed CO_2 and isocynic acid (HN═C═O), or moderately reacted oxygen-containing intermediates products throughout the heating process (Liu et al., 2011; Zhou et al., 2014). Fig. 8(c) represents N 1s spectra. The peak at binding energy 398.0 eV is attributed due to N—C═N or ═NH, another peak at 399.4 eV is corresponds to N—C_3 or —NH— and peak at binding energy 401.4 eV, which is attributed due to C—N—H or —NH^+ group of g-C_3N_4 (Sun et al., 2010b). Fig. 8(d) shows O 1s spectrum containing a peak at binding energy 528.8 eV, which is corresponds to the O^{2-} in TiO_2 and the —OH group on the surface of GNT (Ng et al., 2010). In the Fig. 8(e), two peaks are obtained for Ti 2p spectrum at binding energy 457.4 and 463.3 eV. All the analysis of XPS confirms the successful and proper synthesis of NCs by hydrothermal method.

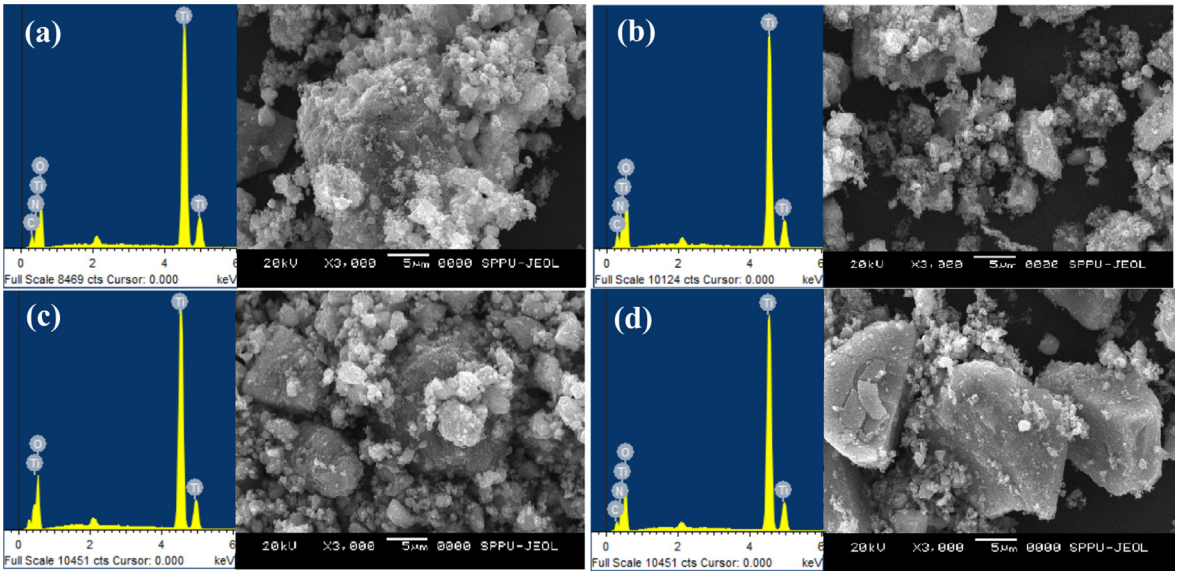

Fig. 6 FE-SEM images and EDAX spectrum of (a) 15-GNT, (b) 30-GNT, (c) TiO_2, (d) M-GNT.

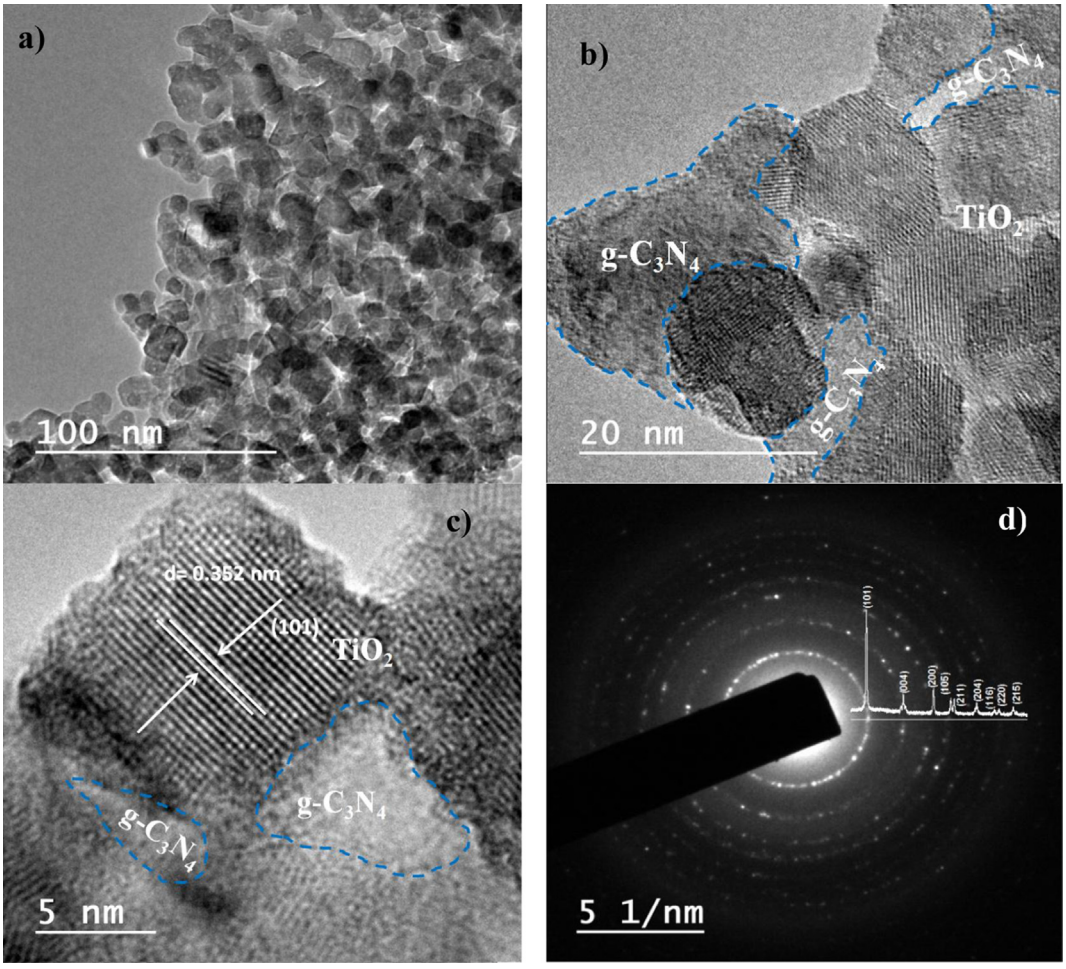

Fig. 7 HR-TEM micrographs of (a) & (b) 15 GNT, (c) 30-GNT, d) SAED pattern of 30-GNT.

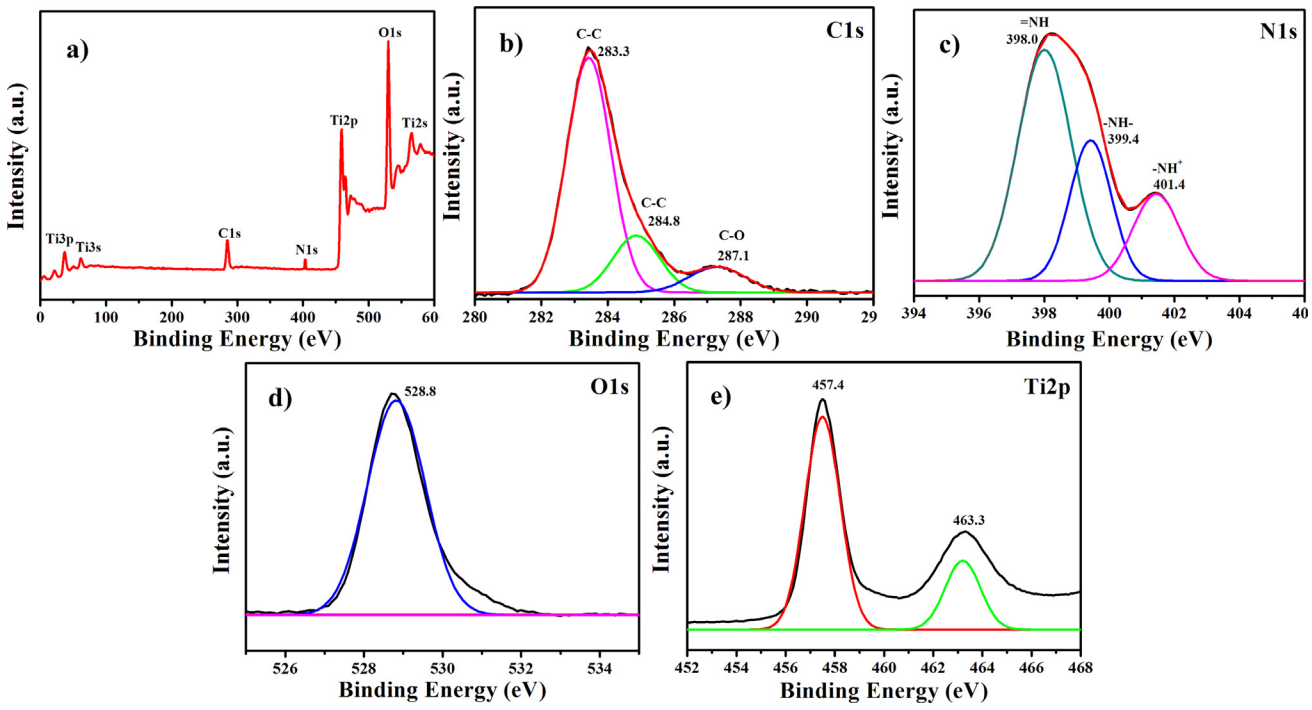

Fig. 8 (a) XPS spectra of GNT, high-resolution spectra of (b) C 1s, (c) N 1s, (d) O 1s, (e) Ti 2p.

4. Photocatalytic activity

The photocatalytic activity of prepared NCs is evaluated for degradation of BG dye, mixture of three dyes (BG, MB and MO) and remerging contaminant BPA. The effect of various parameters such as pH of solution, catalyst composition, catalyst loading and concentration of dye solution on photocatalytic activity is studied thoroughly during degradation reactions.

4.1. Photocatalytic degradation of BG dye

UV–Visible absorption spectra of BG dye in the suspension of 30-GNT composite with respect to irradiation time are shown in Fig. 9(a). As can be seen from the figure, the characteristic absorption peak of BG dye at ~623 nm with other peaks at 420 nm, 310 nm are decrease gradually with respect to time irradiation. The complete degradation of BG dye has been observed after 150 min by using 30-GNTnanocomposite.

Kinetic plot of BG photodegradation reaction for the different catalysts with respect to varying irradiation time is shown in Fig. 9(b). The control of experiments reveals that concentration of BG has been constant in absence of photocatalyst in presence of sunlight, suggest that BG dye is very much stable photochemically. Within irradiation time of 150 min., the complete degradation (~95%) of BG is observed for 30-GNT composite; while 59.82%, 70.40%, 73.74%, 78.67% degradation of BG is noted for M-GNT, g-C_3N_4, TiO_2, 15-GNT, respectively and hence it reveals that 30-GNT required less time to degrade BG completely to that of other composites, bare g-C_3N_4 and bare TiO_2. This observation indicates that the photocatalytic degradation reaction of the composite is highly dependent upon the amount of g-C_3N_4 incorporated

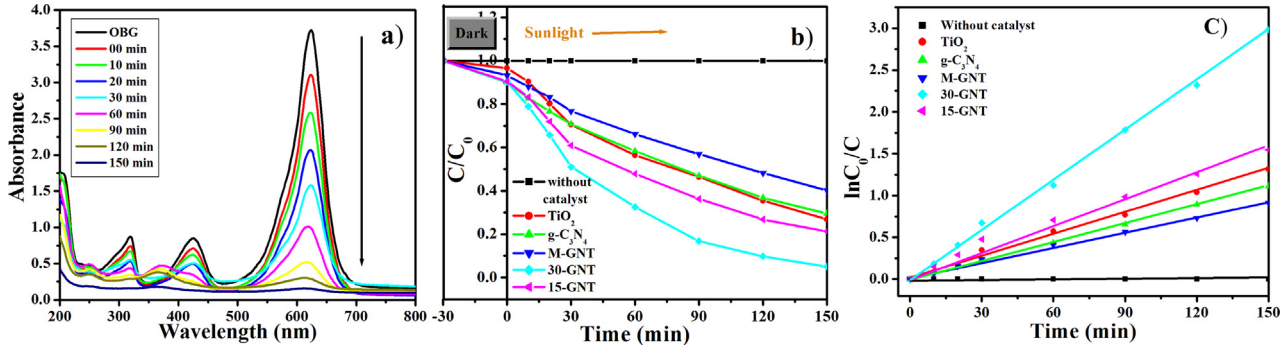

Fig. 9 (a) Optical absorption spectrum of BG, (b) Kinetic plot of BG photodegradation reaction for the different catalysts and (c) corresponding plot of $\ln C_0/C$ vs time [Experimental Conditions: [BG] = 20.0 mg/L, amount of 30-GNT catalysts = 100 mg, volume of solution = 200 ml and aqueous medium].

into TiO_2. Higher activity of 30-GNT as compare to other prepared NC's and bare TiO_2 is because of lower crystallite size and band gap. As discussed in earlier section, 30-GNT having lower average crystallite size i.e. 11.42 nm as compare with other prepared catalysts such as 15-GNT, M-GNT and bare TiO_2 having average crystallite size 12.22 nm, 18.24 nm and 20.13 nm respectively. Furthermore, 30-GNT catalyst having higher photoresponce in visible light, as it shows more absorption in visible region with lowest band gap about 2.9 eV.

In the photodegradation studies, the apparent rate constant was applied usually because it consents for the independent determination of photocatalytic activity of the previous adsorption period. The apparent first order kinetic equation is given as follows:

$$-\log\frac{C_0}{C} = K_{app.}\frac{t}{2.303} \quad (1)$$

where, K_{app} is the apparent rate constant of a reaction, C_0 is the initial concentration of dye solution at t = 0 and C is the remaining concentration of dye solution at time t (Barkul et al., 2016).

Table 2 shows the reaction kinetic parameters for photocatalytic degradation of BG using different NCs, bare g-C_3N_4 and bare TiO_2. As compared to other catalysts, 30-GNT has shown the higher rate constant ($19.85 \times 10^{-3}min^{-1}$) for degradation of BG under direct sunlight and it is almost twice to that of bare TiO_2 and bare g-C_3N_4.

Fig. 9(c) shows plot of lnC_0/C of BG dye in the suspension of all samples with irradiation time. The linear nature of graph of lnC_0/C of all samples with respect to irradiation time, suggest that photocatalytic degradation is first order kinetics (Barkul et al., 2017).

Due to better catalytic activity of 30-GNT, the further photo-degradation studies are carried out using 30-GNT catalyst by varying the other preparative parameters such as concentration of dye, pH of dye solution, amount of catalyst, etc.

Different concentrations of BG dye (15 ppm to 30 ppm) was used to explore the effect on rate of photocatalytic degradation. From the plot of change in concentration of BG per minute with irradiation time (Fig. 10(a)), the photodegradaton rate was found to be increases with increase in the initial concentration of dye from 15 to 25 ppm initial concentration of BG dye. This is due to availability of more number of dye molecules for excitation and degradation. Further increasing the concentration i.e. for 30 ppm solution of BG, rate of degradation remains same or slightly decreased. This is due to the fact that, at more concentration of dye, colour intensity increases; which affects the light intensity passing through the reaction medium to reach the surface of the photocatalyst (Abdellah et al., 2018). Furthermore, the complete degradation of 15 ppm solution can be achieved in 120 min. But for 20, 25 and 30 ppm concentration complete degradation has not been achieved in 120 min., whereas 90, 78 and 67% degradation has been achieved respectively (Fig. 10(b)).

Table 2 Reaction kinetic parameters of photocatalytic degradation of BG using GNT, bare TiO_2 and g-C_3N_4 after irradiation time of 150 min (peak at wavelength ~623 nm).

Name of catalysts	Initial concentration of BG (%)	Remaining concentration of BG after 150 min (%)	Rate constant (min^{-1})
TiO_2	100.0	26.86	9.327×10^{-3}
g-C_3N_4	100.0	29.60	7.725×10^{-3}
M-GNT	100.0	40.18	6.641×10^{-3}
15-GNT	100.0	21.33	12.42×10^{-3}
30-GNT	100.0	5.05	19.85×10^{-3}

The photodegradation efficiency of the reaction greatly depends up on pH of dyes solution. Also, the wastewater from textile, cosmetics, and printing industries contains mixture of dyes, mostly having a wide pH range. Therefore, the optimized results of photodegradation of BG dye by changing pH of dye solution have been illustrated in Fig. 10(c). The rate of reaction is higher in acidic medium (pH 3.0, 5.0) than that of basic medium (pH 11.0, 9.0). The different pH of solution can change the surface charge of GNT composite and change the potential of the photocatalytic reactions. Reactive species $OH^{\cdot}$, $O_2^{\cdot-}$, and $HO_2^{\cdot}$ are responsible for photodegradation. Formation of these reactive species takes place as shown in Eqs. (2)–(5) (Pingmuang et al., 2017). Formation of $HO_2^{\cdot}$ is favoured under acidic condition. Higher degradation rate under acidic condition, shows that $HO_2^{\cdot}$ is main oxidation specie in prepared composite photo catalysis system. In basic and acidic condition of the solution deprotonate and protonate the surface of catalysts respectively. Hence the surface of titania have appear negatively charged in alkaline medium and positively charged in acidic medium. The adsorption of dye on the surface of titania can change the rate of reaction (Rauf and Ashraf, 2009).

$$e^-_{CB} + O_2(aq) \rightarrow O_2^{-\cdot} \quad (2)$$

$$e^-_{CB} + O_2(aq) + H^+ \rightarrow HO_2^{\cdot} \quad (3)$$

$$h^+_{VB} + OH^- \rightarrow OH^{\cdot} \quad (4)$$

$$h^+_{VB} + H_2O \rightarrow H^+ + OH^{\cdot} \quad (5)$$

The photocatalytic degradation efficiency was evaluated by changing catalyst loading of 30-GNT from 0.25 g/L to 1 g/L mg for BG solution and illustrated in Fig. 10(d). The results revealed that the rate of catalytic reaction increases with increase in amount of catalyst loading, as the presence higher amount of catalyst provides the higher active surface area and sites, which are involved in the degradation reaction. Also, due to increase in catalyst loading adsorption of dye on the surface of catalyst also increases. For 0.25 g/L loading the initial adsorption (in dark) of dye on the catalyst surface is about12% and increases to 20% for 1 g/L catalyst loading.

4.2. Photocatalytic degradation of BPA

Photocatalytic studies of the synthesized NCs were tested against the degradation of BPA under sunlight irradiation. Measured absorption spectrum of BPA during photocatalytic studies with relevant irradiation time in presence of 30-GNT is shown in Fig. 11(a). From the figure, absorbance maximum of BPA solution is observed at wavelength ~277 nm. Peak has been gradually decreased with increase in time illumination and complete degradation of BPA occurred in 240 min. Fig. 11(b) shows change in concentration of BPA dye in the suspension of 15-GNT, 30-GNT, M-GNT, TiO_2, g-C_3N_4 and

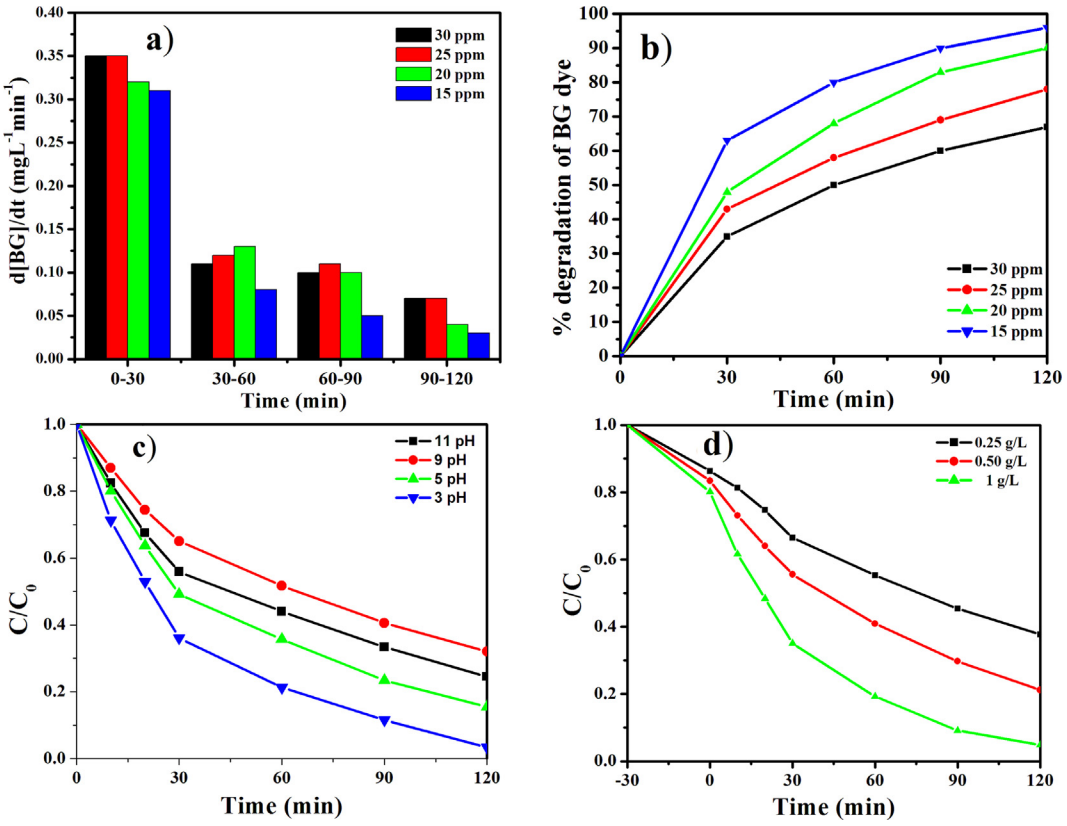

Fig. 10 Plot of (a) d[BG]/dt versus time, (b) percentage degradation of BG dye versus irradiation time (min.) for different concentration of BG dye solution, (c) C/C_0 versus irradiation time (min) for varying pH of dye solution and (d) change in concentration of BG by using 30-GNT with different amount of catalysts with irradiation time.

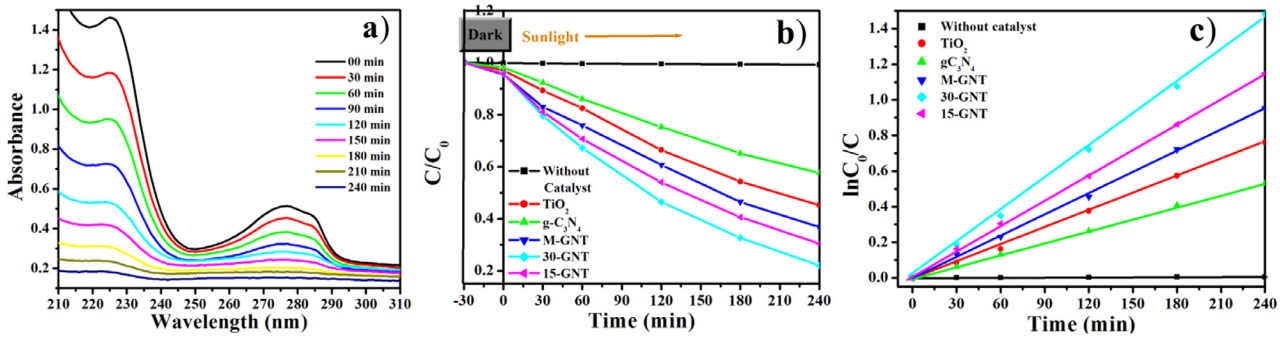

Fig. 11 (a) Absorption measurement of BPA solution by using 30-GNT with irradiation time, (b) Change in concentration of BPA and (c) plot of $\ln C_0/C$ of BPA by using 30-GNT, 15-GNT pure TiO_2, M-GNT and without catalyst with irradiation time. [Experimental Conditions: [BPA] = 20.0 mg/L, amount of catalyst = 100 mg, volume of solution = 200 ml, in aqueous medium].

without catalysts. The control experiment i.e. without using any catalyst, has not shown any degradation of BPA, which suggest that BPA is more stable photochemically. The higher photocatalytic degradation of BPA is observed for 30-GNT in 240 min as compare to other catalysts. Hence, this overall study again confirms that proportion amount of g-C_3N_4 incorporated into TiO_2 have more significant factor in the prepared nanocomposite. The higher efficiency of 30-GNT is due to lower crystallite size and band gap than other catalysts. The plot of linear nature of $\ln C_0/C$ of all photocatalysts with respect to time (Fig. 11(c)), shows that the photocatalytic degradation reaction is first order kinetics. Rate constant for BPA photodegradation study using 30-GNT is twice of using bare TiO_2 under similar experimental conditions (Table 3).

4.3. Photocatalytic degradation of mixed dyes

As per our earlier photodegradation study of BG and BPA, it is concluded that 30-GNT is more effective nanocomposite as compared to other synthesized nanocomposites or bare TiO_2. Hence, photodegradation studies of mixed dye were carried

Table 3 Reaction kinetic parameters of photocatalytic degradation of BPA using GNT, bare TiO_2 and g-C_3N_4 after irradiation time of 240 min (peak at wavelength ~ 277 nm).

Name of catalysts	Initial concentration of BPA (%)	Remaining concentration of BPA after 240 min (%)	Rate constant (min^{-1})
TiO_2	100.0	45.26	15.75×10^{-3}
g-C_3N_4	100.0	57.62	8.127×10^{-3}
M-GNT	100.0	36.73	20.26×10^{-3}
15-GNT	100.0	30.44	24.86×10^{-3}
30-GNT	100.0	21.98	30.32×10^{-3}

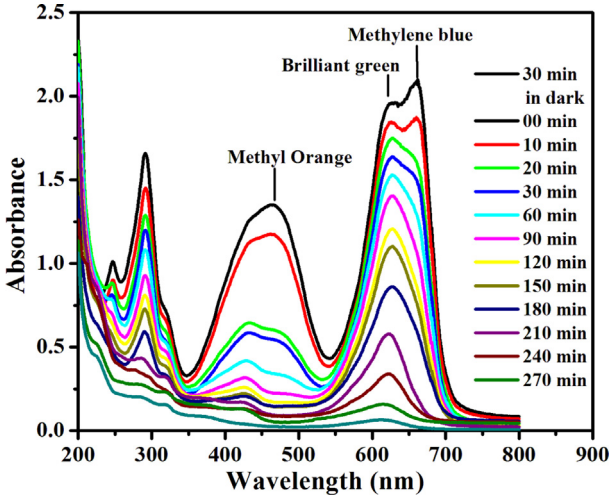

Fig. 12 Absorption spectrum of mixture of dyes by using 30-GNT with irradiation time.

out only by using 30-GNT nanocomposite. Here, we have used aqueous solution of mixture of three dyes namely methyl orange (MO), methylene blue (MB) and brilliant green (MG). The control experiments reveals that the photolysis of MO, BG and MB is very slow without photocatalyst under solar irradiation. Fig. 12 shows change in concentration of mixed dyes (MB, BG and MO) in the suspension of 30-GNT with respect to irradiation time. Absorption peaks are obtained at wavelengths ~464 nm, ~ 624 nm and ~662 nm, which are characteristic absorption peaks (λ_{max}) of MO, BG and MB respectively. Initial concentration of mixed dyes decreases with increase in time illumination and intensity of these peaks gradually decreases. The complete degradation of these dyes in aqueous solution has taken place in 270 min. Overall photodegradation of these dyes confirms that 30-GNT also degrade mixture cationic and anionic dyes under direct sunlight irradiation.

5. Recyclability of catalysts

Reusability of the prepared NC is one the most significant feature for catalyst efficiency over practical reuses. Therefore, three cycles of photocatalytic degradation of BG was carried out using 30-GNT under sunlight and shown in Fig. 13. A result reveals the outstanding efficiency of the catalyst after

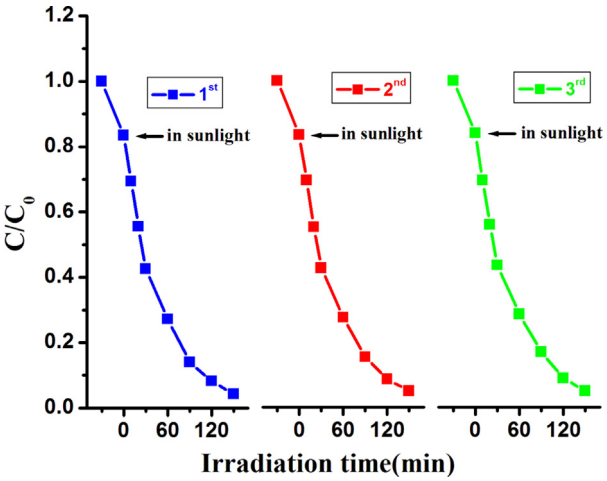

Fig. 13 Catalysts recyclability [Experimental Conditions: [BG] = 20.0 mg/L, amount of 30-GNT catalyst = 100 mg, volume of solution = 200 ml, in aqueous medium].

three cycles and this confirmed the stability of the prepared catalyst.

6. Conclusions

Visible active g-C_3N_4-TiO_2(GNT) NCs were successfully synthesized by using hydrothermal method. Among the various NCs, 30-GNT has shown the better efficiency for photodegradation of brilliant green (BG), bisphenol A (BPA) and mixture of three dyes namely methylene blue (MB), brilliant green (BG) and methyl orange (MO). Furthermore, from the characterisation of the catalysts, it has been confirm that g-C_3N_4 act as a sensitizer in the photocatalytic degradation. However, strong interaction of g-C_3N_4 with TiO_2 has been proved by FTIR and Raman analysis. From UV–Visible absorption study, 30-GNT catalyst has shown better visible light absorption than other catalysts. The band gap 2.9, 3.0, 3.16 and 3.3 eV has been observed for 30-GNT, 15-GNT, M-GNT and bare TiO_2 respectively. Also, 30-GNT catalyst has been shown almost similar efficiency for three cycles. Rate constant of 30-GNT catalyst is twice to that of bare TiO_2 for degradation of brilliant green dye and bisphenol A.

Declaration of Competing Interest

The authors confirm that this article content has no conflict of interest.

Acknowledgement

RSS deeply acknowledges to University Grants Commission (UGC), New Delhi, India for providing Senior Research Fellowship (Ref. No. 22/12/2013(ii) EU-V and Sr. No. 2121310321).

References

Abdellah, M.H., Nosier, S.A., El-Shazly, A.H., Mubarak, A.A., 2018. Photocatalytic decolorization of methylene blue using TiO_2/UV system enhanced by air sparging. Alexandria Eng. J. 57, 3727–3735.

Barkul, R.P., Koli, V.B., Shewale, V.B., Patil, M.K., Delekar, S.D., 2016. Visible active nanocrystalline N-doped anatase TiO_2 particles

for photocatalytic mineralization studies. Mater. Chem. Phys. 173, 42–51.
Barkul, R.P., Patil, M.K., Patil, S.M., Shevale, V.B., Delekar, S.D., 2017. Sunlight-assisted photocatalytic degradation of textile effluent and rhodamine b by using iodine doped TiO_2 nanoparticles. J. Photochem. Photobiol. A. 349, 138–147.
Cui, W., Chen, L., Sheng, J., Li, J., Wang, H., Dong, X., Zhou, Y., Sun, Y., Dong, F., 2020. The pivotal roles of spatially separated charge localization centers on the molecules activation and photocatalysis mechanism. Appl. Catal. B. Environ. 262, 118251.
Dai, H., Zhang, S., Xu, G., Peng, Y., Gong, L., Li, X., Li, Y., Lin, Y., Chen, G., 2014. Highly photoactive heterojunction based on g-C_3N_4 nanosheets decorated with dendritic zinc (II) phthalocyanine through axial coordination and its ultrasensitive enzyme-free sensing of choline. RSC Adv. 4, 58226–58230.
Ding, Z., Chen, X., Antonietti, M., Wang, X., 2011. Synthesis of transition metal-modified carbon nitride polymers for selective hydrocarbon oxidation. Chem. Sus. Chem. 4, 274–281.
Fu, G., Vary, P.S., Lin, C.-T., 2005. Anatase TiO_2 nanocomposites for antimicrobial coatings. The J. Phys. Chem. B 109, 8889–8898.
Fujishima, A., Honda, K., 1972. Electrochemical photolysis of water at a semiconductor electrode. Nature 238, 37.
Ge, L., Han, C., Xiao, X., Guo, L., Li, Y., 2013. Enhanced visible light photocatalytic hydrogen evolution of sulfur-doped polymeric g-C_3N_4 photocatalysts. Mater. Res. Bull. 48, 3919–3925.
Gondal, M., Adesida, A., Rashid, S., Shi, S., Khan, R., Yamani, Z., Shen, K., Xu, Q., Seddigi, Z.S., Chang, X., 2015. Preparation of WO_3/g-C_3N_4 composites and their enhanced photodegradation of contaminants in aqueous solution under visible light irradiation. Reac. Kinet. Mech. Catal. 114, 357–367.
Guo, Q., Xie, Y., Wang, X., Lv, S., Hou, T., Liu, X., 2003. Characterization of well-crystallized graphitic carbon nitride nanocrystallites via a benzene-thermal route at low temperatures. Chem. Phys. Lett. 380, 84–87.
Henderson, M.A., 2011. A surface science perspective on TiO_2 photocatalysis. Surf. Sci. Reports 66, 185–297.
Hoffmann, M.R., Martin, S.T., Choi, W., Bahnemann, D.W., 1995. Environmental applications of semiconductor photocatalysis. Chem. Rev. 95, 69–96.
Jun, Y.S., Park, J., Lee, S.U., Thomas, A., Hong, W.H., Stucky, G.D., 2013. Three-dimensional macroscopic assemblies of low-dimensional carbon nitrides for enhanced hydrogen evolution. Angew. Chem. Int. Ed. 52, 11083–11087.
Kubacka, A., Fernandez-Garcia, M., Colon, G., 2011. Advanced nanoarchitectures for solar photocatalytic applications. Chem. Rev. 112, 1555–1614.
Li, H., Bian, Z., Zhu, J., Huo, Y., Li, H., Lu, Y., 2007. Mesoporous Au/TiO_2 nanocomposites with enhanced photocatalytic activity. J. Am. Chem. Soc. 129, 4538–4539.
Liao, J., Cui, W., Li, J., Sheng, J., Wang, H., Dong, X., Chen, P., Jiang, G., Wang, Z., Dong, F., 2020. Nitrogen defect structure and NO^+ intermediate promoted photocatalytic NO removal on H_2 treated g-C_3N_4. Chem. Eng. J. 379, 122282.
Liu, J., Zhang, T., Wang, Z., Dawson, G., Chen, W., 2011. Simple pyrolysis of urea into graphitic carbon nitride with recyclable adsorption and photocatalytic activity. J. Mater. Chem. 21, 14398–14401.
Ma, J., Wang, C., He, H., 2016a. Enhanced photocatalytic oxidation of NO over g-C_3N_4-TiO_2 under UV and visible light. Appl. Catal. B. Environ. 184, 28–34.
Ma, L., Fan, H., Wang, J., Zhao, Y., Tian, H., Dong, G., 2016b. Water-assisted ions in situ intercalation for porous polymeric graphitic carbon nitride nanosheets with superior photocatalytic hydrogen evolution performance. Appl. Catal. B. Environ. 190, 93–102.
Marugán, J., Van Grieken, R., Alfano, O.M., Cassano, A.E., 2006. Optical and physicochemical properties of silica-supported TiO_2 photocatalysts. AIChE J. 52, 2832–2843.
Ng, J., Xu, S., Zhang, X., Yang, H.Y., Sun, D.D., 2010. Hybridized nanowires and cubes: a novel architecture of a heterojunctioned TiO_2/$SrTiO_3$ thin film for efficient water splitting. Adv. Funct. Mater. 20, 4287–4294.
Pan, X., Zhao, Y., Liu, S., Korzeniewski, C.L., Wang, S., Fan, Z., 2012. Comparing graphene-TiO_2 nanowire and graphene-TiO_2 nanoparticle composite photocatalysts. ACS Appl. Mater. interfaces 4, 3944–3950.
Pingmuang, K., Chen, J., Kangwansupamonkon, W., Wallace, G.G., Phanichphant, S., Nattestad, A., 2017. Composite photocatalysts containing $BiVO_4$ for degradation of cationic dyes. Sci. Rep. 7, 8929.
Program, N.B.E., 2017. State of Narragansett Bay and Its Watershed: Summary Report. Narragansett Bay Estuary Program.
Rauf, M., Ashraf, S.S., 2009. Fundamental principles and application of heterogeneous photocatalytic degradation of dyes in solution. Chem. Eng. J. 151, 10–18.
Samanta, S., Martha, S., Parida, K., 2014. Facile synthesis of Au/g-C_3n_4 Nanocomposites: An inorganic/organic hybrid plasmonic photocatalyst with enhanced hydrogen gas evolution under visible-light irradiation. Chem. Cat. Chem. 6, 1453–1462.
Sankar, R., Manikandan, P., Malarvizhi, V., Fathima, T., Shivashangari, K.S., Ravikumar, V., 2014. Green synthesis of colloidal copper oxide nanoparticles using Carica papaya and its application in photocatalytic dye degradation. Spectrochim. Acta A. Mol. Biomol. Spectrosc. 121, 746–750.
Schwinghammer, K., Mesch, M.B., Duppel, V., Ziegler, C., Senker, Jr, Lotsch, B.V., 2014. Crystalline carbon nitride nanosheets for improved visible-light hydrogen evolution. J. Am. Chem. Soc. 136, 1730–1733.
Shao, L., Jiang, D., Xiao, P., Zhu, L., Meng, S., Chen, M., 2016. Enhancement of g-C_3N_4 nanosheets photocatalysis by synergistic interaction of ZnS microsphere and RGO inducing multistep charge transfer. Appl. Catal. B. Environ. 198, 200–210.
Sridharan, K., Jang, E., Park, T.J., 2013. Novel visible light active graphitic C_3N_4–TiO_2 composite photocatalyst: synergistic synthesis, growth and photocatalytic treatment of hazardous pollutants. Appl. Catal. B. Environ. 142, 718–728.
Sun, H., Wang, S., Ang, H.M., Tadé, M.O., Li, Q., 2010a. Halogen element modified titanium dioxide for visible light photocatalysis. Chem. Eng. J. 162, 437–447.
Sun, Y., Li, C., Xu, Y., Bai, H., Yao, Z., Shi, G., 2010b. Chemically converted graphene as substrate for immobilizing and enhancing the activity of a polymeric catalyst. Chem. Commun. 46, 4740–4742.
Takanabe, K., Kamata, K., Wang, X., Antonietti, M., Kubota, J., Domen, K., 2010. Photocatalytic hydrogen evolution on dye-sensitized mesoporous carbon nitride photocatalyst with magnesium phthalocyanine. Phys. Chem. Chem. Phys. 12, 13020–13025.
Troppová, I., Šihor, M., Reli, M., Ritz, M., Praus, P., Kočí, K., 2018. Unconventionally prepared TiO_2/g-C_3N_4 photocatalysts for photocatalytic decomposition of nitrous oxide. Appl. Surf. Sci. 430, 335–347.
Wang, H., He, W., Dong, X., Wang, H., Dong, F., 2018. In situ FT-IR investigation on the reaction mechanism of visible light photocatalytic NO oxidation with defective g-C_3N_4. Sci. Bull. 63, 117–125.
Wang, Y., Shi, R., Lin, J., Zhu, Y., 2011. Enhancement of photocurrent and photocatalytic activity of ZnO hybridized with graphite-like C_3N_4. Energy Environ. Sci. 4, 2922–2929.
Xing, C., Wu, Z., Jiang, D., Chen, M., 2014. Hydrothermal synthesis of In_2S_3/g-C_3N_4 heterojunctions with enhanced photocatalytic activity. J. Colloid Interface Sci. 433, 9–15.
Xiong, T., Wang, H., Zhou, Y., Sun, Y., Cen, W., Huang, H., Zhang, Y., Dong, F., 2018. KCl-mediated dual electronic channels in layered g-C_3N_4 for enhanced visible light photocatalytic NO removal. Nanoscale 10, 8066–8074.

Yang, F., Yan, N.-N., Huang, S., Sun, Q., Zhang, L.-Z., Yu, Y., 2012. Zn-doped CdS nanoarchitectures prepared by hydrothermal synthesis: mechanism for enhanced photocatalytic activity and stability under visible light. J. Phys. Chem. C 116, 9078–9084.

Yang, S., Gong, Y., Zhang, J., Zhan, L., Ma, L., Fang, Z., Vajtai, R., Wang, X., Ajayan, P.M., 2013. Exfoliated graphitic carbon nitride nanosheets as efficient catalysts for hydrogen evolution under visible light. Adv. mater. 25, 2452–2456.

Zhang, Y., Gong, H., Li, G., Zeng, H., Zhong, L., Liu, K., Cao, H., Yan, H., 2017. Synthesis of graphitic carbon nitride by heating mixture of urea and thiourea for enhanced photocatalytic H_2 production from water under visible light. Int. J. Hydrogen Energy 42, 143–151.

Zhao, H.-M., Di, C.-M., Wang, L., Chun, Y., Xu, Q.-H., 2015. Synthesis of mesoporous graphitic C_3N_4 using cross-linked bimodal mesoporous SBA-15 as a hard template. Microporous Mesoporous Mater. 208, 98–104.

Zhou, J., Zhang, M., Zhu, Y., 2015. Photocatalytic enhancement of hybrid C_3N_4/TiO_2 prepared via ball milling method. Phys. Chem. Chem. Phys. 17, 3647–3652.

Zhou, S., Liu, Y., Li, J., Wang, Y., Jiang, G., Zhao, Z., Wang, D., Duan, A., Liu, J., Wei, Y., 2014. Facile in situ synthesis of graphitic carbon nitride (g-C_3N_4)-N-TiO_2 heterojunction as an efficient photocatalyst for the selective photoreduction of CO_2 to CO. Appl. Catal. B. Environ. 158, 20–29.